Indoor off-body wireless MIMO communication with dual polarized textile antennas

Patrick Van Torre, Luigi Vallozzi, Carla Hertleer,
Hendrik Rogier, *Senior Member IEEE*, Marc Moeneclaey, *Fellow IEEE*, Jo Verhaevert

***Abstract*—Off-body data communication for firefighters and other rescue workers is an important area of development. The communication with a moving person in an indoor environment can be very unreliable due to channel fading. In addition, when considering off-body communication by means of textile antennas, propagation is affected by shadowing caused by the human body. By transmitting and receiving signals using multiple-input, multiple-output antennas (MIMO communication) a large improvement in reliability of the wireless link is obtained. In this contribution, the performance of wireless data communication using quadrature phase shift keyed (QPSK) modulated data in the 2.45 GHz ISM-band is evaluated in the case of firefighters walking indoor and communicating by means of a compact dual-pattern dual-polarization diversity textile patch antenna system integrated into their clothing. Simultaneous transmit diversity (at the firefighter) and receive diversity (at the base station) up to fourth order are achieved by means of orthogonal space-time codes, providing a maximum total diversity order of 16.**

The measurements confirm that MIMO techniques drastically improve the reliability of the wireless link. Measurements are compared for three test persons of significantly different sizes. For equal transmitted power levels, the bit error rates for the 2×2 and 4×4 links are much lower than for a system without diversity, with the 4×4 system clearly providing the best performance.

***Index Terms*—body-centric, diversity, ISM band, multiple-input multiple-output (MIMO) systems, space-time codes, textile antennas**

I. Introduction

The performance of a multiple-input multiple-output (MIMO) wireless off-body data communication link is studied for the case of a firefighter working in a building and communicating by means of multiple textile patch antennas integrated in his/her clothing. Earlier measurement campaigns, involving a single transmit antenna at the base station and multiple receive antennas in the garment of the moving firefighter, were performed by our team in the same environment. These scenarios achieved second-order receiver diversity [1] and fourth-order receiver diversity at the firefighter using two dual-polarized antennas [2]. However, this paper discusses our first measurement campaign using true MIMO communication, combining transmit diversity at the firefighter (using space-time codes sent over textile antennas) and receive diversity at the base station. Bit error rates documenting the real-time behavior of an actual data transmission are presented.

Recent measurement campaigns related to body-centric wireless communication with multiple antennas have been documented in [3]–[17] but to our knowledge, no measurements transmitting real blocks of data off-body, via a textile antenna system, over a 4×4 MIMO communications link have been published before.

The 2.45 GHz ISM frequency band was chosen for the transmissions, providing a sufficiently large bandwidth and allowing to design antennas of a convenient size, given the wavelength of 12cm. The integration of textile antennas in the garment is not straightforward, as the equipment carried by the firefighter severely limits the number of suitable locations for an antenna.

The indoor environment consists of a fading channel where multipath effects and shadowing make the signal levels fluctuate significantly as a function of position. Channel measurements in the same environment revealed Rayleigh type small-scale fading. Using multiple antennas and combining the received signals by means of diversity techniques significantly improves the performance of the wireless link. The use of multiple antennas is also very effective against degradation of the communication due to the shadowing effect of the human body. Using two dual polarized textile antennas, on the front and back of the firefighter, fourth order diversity is realized using only two patch antennas. The base station uses the same type of antennas, placed one meter apart, and also achieves fourth-order diversity. The resulting 4×4 MIMO channel provides a maximum total diversity order of 16. The measurements in this paper pertain to the situation where the firefighter is transmitting data to the base station.

Sections II-III document the measurement setup and results. At the transmitter, a sequence of uncoded QPSK symbols enters a space-time encoder, whose outputs are applied to N_t antenna ports. The received signals, captured by N_r antenna ports, are properly combined according to the particular space-time code, making use of the estimated channel gains. In our experimental setup we consider $N_t = N_r = N$ (being the most realistic situation for a bidirectional wireless link), with $N = 1, 2, 4$. The resulting signal to noise ratios (SNRs) at the detector and the associated bit error rates (BERs) clearly demonstrate the advantages of MIMO communication.

H. Rogier, L. Vallozzi and P. Van Torre are with the Information Technology Department (INTEC), Ghent University, St. Pietersnieuwstraat 41, 9000 Ghent, Belgium. E-mails: Hendrik.Rogier@UGent.be Luigi.Vallozzi@UGent.be Patrick.VanTorre@UGent.be

M. Moeneclaey is with the Department of Telecommunications and Information Processing (TELIN), Ghent University, St. Pietersnieuwstraat 41, 9000 Ghent, Belgium. E-mail: Marc.Moeneclaey@UGent.be

C. Hertleer is with the Department of Textiles, Ghent University, 9052 Zwijnaarde, Belgium. E-mail: Carla.Hertleer@UGent.be

J. Verhaevert en P. Van Torre are with Hogeschool Gent, INWE department, Schoonmeersstraat 52, 9000 Gent, Belgium

In a real-life scenario, the effective diversity for the practical range of signal-to-noise ratios is degraded by the correlation between the signals and by unequal channel gain. The impact of antenna coupling on MIMO communication has been studied in [3] and specifically for dual-polarized antennas in [4]. Channel measurements with dual polarized transmissions are presented in [5]; in our measurements the polarization of the off-body antennas varies, due to changes in body posture of the rescue worker in action. The correlation of signals received by dual polarized antennas in an indoor environment was studied in [17]. In [14] measurements of a body-worn antenna system are performed in open space and the effects of a multipath environment are indirectly assessed.

By means of the cumulative distribution function for the instantaneous SNR at the detector input we compare the 10% outage probability levels for the 1×1, 2×2 and 4×4 systems. The corresponding bit error characteristics resulting from the measurement are compared to the theoretical BER characteristics for independent identically distributed Rayleigh fading channels. The measured correlation between the signal levels for different antennas and polarizations indicates to which degree the channels vary independently.

In Section IV, the channel is modeled using the Kronecker and Eigenbeam channel models. Based on these models, the BER characteristics are accurately regenerated using a matrix of i.i.d. pseudo random values having the same statistical distribution as the measured signals. The differences in distribution have a significant impact on BER characteristics, as shown theoretically in [18] for Nakagami distributed signals.

Additional measurements with three test persons of significantly different sizes are presented in Section V, resulting in similar performance gains by using MIMO communication. Due to the nature of the measurements, with a real test person performing a random walk in an active office environment during working hours; each measurement session will always be different. Despite this variation, the use of diversity techniques always results in a significant performance gain.

II. Measurement details

A. Measurement setup

We consider the uplink scenario, where the mobile firefighter transmits and the base station receives. The measurement setup is composed of two fixed dual-polarized patch antennas connected to the base station, resulting in a total of four received signals. The wearable antenna system under test consists of two similar dual-polarized textile antennas, resulting in four simultaneously transmitted signals. The proposed wearable antenna system is realized by integrating two textile antennas, as documented in Section II-B, into the front and back side of a firefighter jacket, worn by a test person, as shown in Fig. 1. All antennas are then connected to a Signalion-HaLo 430 measurement testbed, operated by our Matlab software. The transmitted space-time encoded data blocks consist of QPSK symbols, modulated on an RF carrier frequency of 2.45 GHz at a baud rate of 1 Msymbols/s. The corresponding complex baseband signals are generated in Matlab and then up converted to RF by the testbed transmitter.

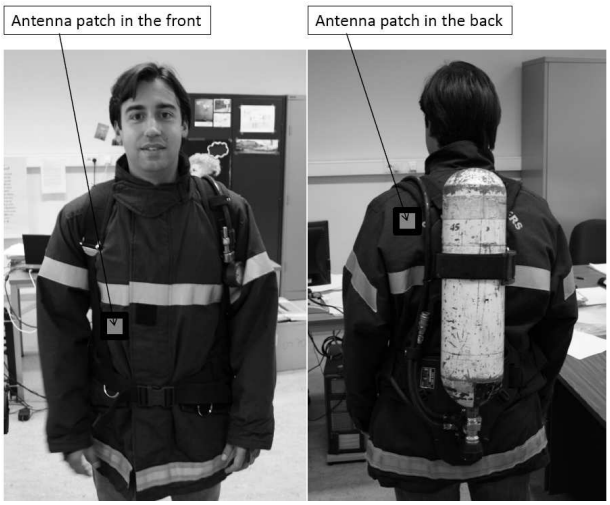

Fig. 1. Positions of front (ports 1,2) and back (ports 3,4) transmitting antennas integrated into the firefighter jacket (on the inside, the antennas are actually not visible).

The testbed receiver down converts to baseband the signals received by the textile antenna system and samples the resulting baseband signals. These samples are post-processed in Matlab, in order to perform carrier frequency offset estimation and correction, timing estimation and correction, channel estimation, space-time decoding, demapping and calculation of BERs and SNRs.

B. Wearable textile antennas

In this measurement, dual-polarized textile patch antennas are used [19], enabling the implementation of 4^{th}-order diversity in a compact dual-pattern dual-polarized system.

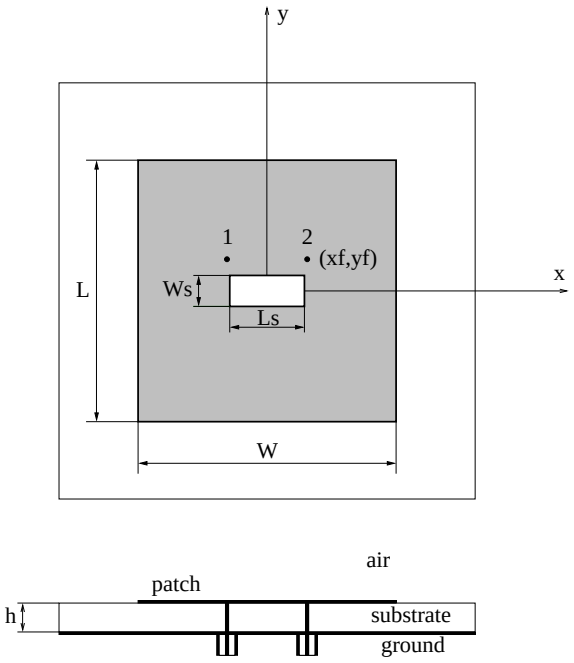

Fig. 2. Layout of the textile antenna with two feed points, to excite signals with orthogonal quasi-linear polarizations.

The dual-polarized wearable antenna, shown in Fig. 2, is a patch antenna consisting entirely of textile materials, suitable for integration into protective clothing such as firefighter suits. The substrate material is a protective, water-repellent, fire-retardant foam, commonly used in firefighter garments, whereas the ground plane and patch are made out of FlecTron® and ShieldIt® respectively, two breathable and highly conductive textile materials.

The layout of the dual-polarized patch antenna consists of a rectangular patch with a slot. The antenna possesses two feed points, each one corresponding to an antenna terminal or port, located on the patch diagonals. The topology and feeding structure ensure the excitation of two signals with different polarizations. The wearable antenna, at center frequency $f = 2.45$ GHz, was designed to transmit/receive two quasi-linearly polarized waves, which are almost orthogonal in space, with the two polarizations oriented at tilt angles of about $\alpha = \pm 45°$. The radiation pattern of the antenna has been verified by measurement in the anechoic chamber [2]. The antenna radiates most of its power away from the body and approximately covers a half-space.

The transmitting patch antenna is located in the firefighter's jacket and aligned for polarizations of +45° and -45° when the user is in the vertical position. Applying two such dual-polarized antennas, one at the front and one at the back of the test person, adds front-to-back diversity, allowing a total of four signals to be transmitted.

Front-to-back diversity is very important in body-centric communications since the human body shadows the RF signals significantly, causing the front and back antennas to virtually cover two complementary half-spaces [1], [2].

C. The indoor environment

A floor plan of the indoor environment where the measurements were performed is displayed in Fig. 3. The path followed by the test person during the measurements is marked, as well as the position of the receiver.

The considered cases are listed here as a function of the labels shown on Fig. 4 in Section III-A.

1) Path $A_1 \rightarrow B_1$: the test person walking towards the receiver from a distance of 15 m and ending at 3 m from the receiver.
2) Path $B_1 \rightarrow A_2$: walking away from the receiver, in the opposite direction of the first path.
3) Path $A_2 \rightarrow C_1 \rightarrow A_3$: walking sideways, along a path perpendicular to the receiver, at up to 18 m of distance.

In the first two cases, a line-of-sight path is present to a varying degree. In case 3, the receiving conditions are most unfavorable, since the transmitted signals experience many obstacles and the transmitter-receiver distance is large. The measurements in this article focus mainly on the sideways path in case 3, as previous measurements [1], [2] have clearly confirmed the weak signals in this area and the Rayleigh-like fading due to multipath propagation.

D. Operation of transmitter and receiver

In the MIMO link considered, the firefighter simultaneously transmits four signals in the same frequency range. The receiver synchronously captures these signals on its four antenna ports.

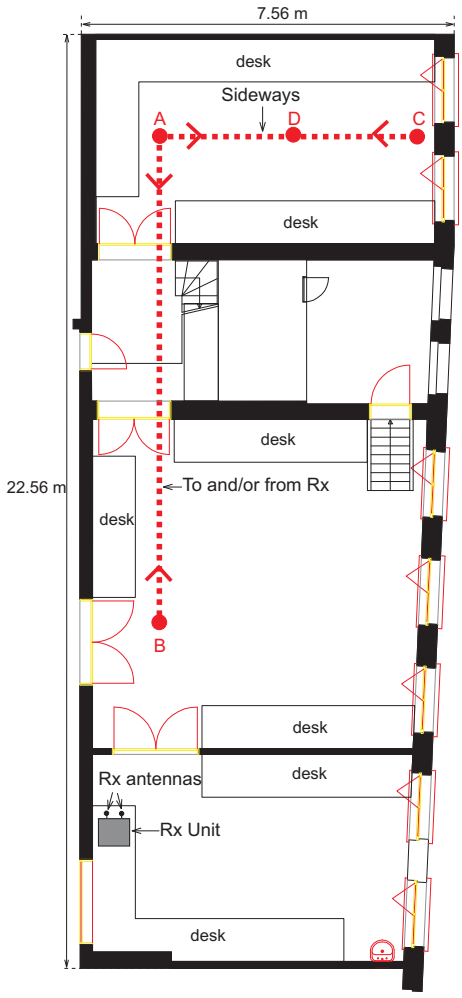

Fig. 3. Floor plan of the multipath environment. The sideways path is Non Line-of-Sight.

In a space-time coded MIMO system with N_r receive and N_t transmit antenna ports, the received signal corresponding to a codeword $\mathbf{C}$ can be represented as

$$\mathbf{R} = \mathbf{HC} + \mathbf{W} \tag{1}$$

where $\mathbf{R}$, $\mathbf{H}$, $\mathbf{C}$, and $\mathbf{W}$ are matrices of dimensions $N_r \times K$, $N_r \times N_t$, $N_t \times K$ and $N_r \times K$, respectively; with K equal to the number of time slots in the codeword. The quantity $h_{m,n} = (\mathbf{H})_{m,n}$ is the complex channel gain between the m-th receive and n-th transmit antenna port; $\mathbf{C}$ is a space-time matrix with orthogonal rows, whose elements are linear functions of L information symbols and their complex conjugates. The information symbols are QPSK symbols, with variance σ_s^2. The elements of the noise matrix $\mathbf{W}$ are i.i.d. complex-valued Gaussian random variables; their real and imaginary parts are independent and have variance $N_0/2$. The quantity $r_{m,k} = (\mathbf{R})_{m,k}$ denotes the signal captured by the m-th receive antenna port during the k-th time slot of duration T.

In our measurement setup, we restrict our attention to $N_r = N_t = N$, with $N = 1, 2, 4$.

- $N = 1$: All quantities in (1) are scalars, with $\mathbf{C}$ reducing to a single QPSK information symbol.
- $N = 2$: We use the Alamouti code [20], defined as

$$\mathbf{C}_2 = \begin{bmatrix} s_1 & -s_2^* \\ s_2 & s_1^* \end{bmatrix}$$

which depends on two QPSK information symbols s_1 and s_2.

- $N = 4$: we use a rate $3/4$ complex orthogonal space-time code [21, pp 194 (5.143)], defined as

$$\mathbf{C}_4 = \begin{bmatrix} s_1 & s_2 & s_3 & 0 \\ -s_2^* & s_1^* & 0 & s_3 \\ s_3^* & 0 & -s_1^* & s_2 \\ 0 & s_3^* & -s_2^* & -s_1 \end{bmatrix}$$

which depends on three QPSK information symbols s_1, s_2 and s_3.

The corresponding total (sum over all transmit antennas) transmit power P_{tr}, total transmitted energy $E_{b,tr}$ per information bit and information bitrate R_b are given in Table I. Note that, for the considered $N \times N$ configurations, we obtain $E_{b,tr} = \sigma_s^2 N/2$.

TABLE I
TRANSMITTED POWER, BITRATE AND ENERGY PER BIT.

N	P_{tr}	R_b	$E_{b,tr} = P_{tr}/R_b$
1	σ_s^2/T	$2/T$	$\sigma_s^2/2$
2	$2\sigma_s^2/T$	$2/T$	σ_s^2
4	$3\sigma_s^2/T$	$3/(2T)$	$2\sigma_s^2$

For a QPSK constellation, the total instantaneous received energy per information bit equals $E_{b,tr} \|\mathbf{H}\|^2 / N$ with $\|\mathbf{H}\|$ denoting the Frobenius norm of $\mathbf{H}$. Similarly, the per antenna port received energy per information bit is $E_{b,tr} \|\mathbf{H}\|^2 / N^2$. The corresponding average energies per information bit are $E_{b,tr} E[\|\mathbf{H}\|^2]/N$ (total) and $E_{b,tr} E[\|\mathbf{H}\|^2]/N^2$ (per receive antenna port).

By linearly combining the quantities $r_{m,k}$, the receiver constructs decision variables on which symbol-by-symbol decision is performed to obtain the detected information symbols. The decision variable z_i related to the information symbol s_i can be decomposed as $z_i = s_i + n_i$ where the noise n_i is a complex-valued Gaussian random variable with i.i.d. real and imaginary parts. For the above cases $N = 1, 2, 4$ the corresponding instantaneous SNR at the detector is given by

$$SNR_D(\mathbf{H}) = \frac{E\left[|s_i|^2\right]}{E\left[|n_i|^2\right]} = \frac{\sigma_s^2}{N_0} \|\mathbf{H}\|^2 = \frac{2E_{b,tr}}{N_0} \frac{\|\mathbf{H}\|^2}{N}. \quad (2)$$

The resulting instantaneous BER for QPSK information symbols [22] is given by

$$BER(\mathbf{H}) = Q(\sqrt{SNR_D(\mathbf{H})}). \quad (3)$$

For a fair comparison, the values of σ_s^2 for the 1×1, 2×2 and 4×4 configurations are adjusted such that the total transmitted power P_{tr} is the same for all configurations

To compare the performance of different MIMO schemes in similar conditions, bursts are transmitted that contain a sequence of data blocks using the following structure:

- A transmission without diversity, using only one of the polarizations on the front antenna (1 TX signal)
- The Alamouti space-time code for pattern diversity using one of the polarizations on both front and back antenna (2 TX signals, F/B: front-to-back diversity)
- The Alamouti space-time code for polarization diversity on the front antenna (2 TX signals)
- The rate $3/4$ space-time code (4 TX signals).

The signals, transmitted simultaneously on multiple antennas, are received on up to four antenna ports. An estimation of the complex-valued channel gains $h_{m,n}$ is performed for all 16 combinations of (m, n). These channel gain estimates are needed to compute the decision variables by properly combining the demodulated signals. The received bit stream is obtained by symbol-by-symbol detection on the decision variables, followed by demapping.

In order to perform the initial estimation of the 16 channels, pilot symbols are transmitted by the four antennas, without overlap in time. These pilots are also used to determine the different carrier frequency offsets for the signals received from different transmit antennas.

TABLE II
STRUCTURE OF THE TRANSMITTED SIGNALS, INDICATING TIMING OF (P)ILOT AND (D)ATA TRANSMISSION.

					1×1	2×2 pol.	2×2 F/B	4×4
TX1	P				D	D	D	D
TX2		P				D		D
TX3			P				D	D
TX4				P				D

Table II illustrates the structure of the transmitted signals. The signals consist of 300 BPSK pilot symbols and 396 QPSK information symbols per transmit antenna for each data block. In our experiment a large overhead is created by transmitting the pilot symbols, because for measurement purposes an accurate channel estimation is preferred. Further tracking of the time-varying channel (during the course of the data burst) is performed using decision oriented feedback.

III. MEASUREMENT RESULTS

The signal levels and bit error rates in Section III-A result from a total transmit power $P_{tr} = 0.1mW$. The power was chosen very low, in order to generate an illustrative amount of bit errors during the measurement.

The results from Sections III-B, III-D and III-E are derived from accurate channel measurements. To minimize the influence of the background noise, the total transmitted power was raised to $100mW$, during an additional set of measurements along the sideways path (case 3).

A. Signal levels and bit error rates

The recorded instantaneous SNRs for each of the 16 channels of the 4×4 transmission are displayed in Fig. 4. The SNR related to the channel from the n-th transmitting port to the m-th receiving port is defined as $SNR = \sigma_p^2 |h_{m,n}|^2 / N_0$, where σ_p^2 denotes the variance of the pilot symbols.

Along the line-of-sight path of cases 1 and 2, the difference in signal levels for transmissions from the front and back antennas is clearly visible. When the firefighter is walking towards the receiver, the signals from the front antenna are significantly stronger than those from the back antenna.

The opposite is true when the firefighter is walking away from the receiver. This illustrates the complementarity of the antennas, with their radiation patterns pointing in opposite directions and their isolation by the shadowing of the body.

In the same graph the BER per burst is displayed for each type of diversity listed in the previous section (the BER plots are listed in the same order). This graph is included as an illustration of the actual wireless MIMO link in operation. The total transmitted power is constant for all diversity types; $100\mu W$ for the 1×1 link, $50\mu W$ per antenna for the 2×2 links and $25\mu W$ per antenna for the 4×4 link.

The following considerations are important for a correct interpretation of the graph:

- The signal levels plotted for each burst are calculated based on the average received power during the transmission of the pilot symbols. This is only an estimate of the received SNR, as the channels are not invariant during the transmission of the burst.
- The signal levels vary drastically during the measurement, due to the path walked by the firefighter. Although this is useful to demonstrate the shadowing effect of the body in the to/from cases, there is also a downside. As the bit errors result from a single implementation based on a limited number of bursts, the bit error rates in this particular graph only indicate the order of magnitude of the statistical BER to be expected with the type of diversity used.
- The performance of the detection at very low signal levels is compromised by inaccurate channel estimation, due to the small transmit power and the limited number of pilot symbols per burst.
- For all of the above reasons the graph fails to point out the better performance of 2nd order (at the transmitter) front-to-back over polarization diversity, as the BER values for both cases are in the same order of magnitude. A more accurate comparison with calculated BER characteristics is deferred to section III-E.

For the 1×1 configuration (no diversity), errors occur even along the line-of-sight path (cases 1 and 2), in spite of strong average signal levels. Along this path no errors occur when using 2×2 or 4×4 MIMO systems transmitting the same power.

Further, even in this short measurement series, the superiority of the 4×4 MIMO link over both 2×2 systems is illustrated by the lower BER values recorded along the sideways path (non line-of-sight; case 3).

B. Cumulative distribution functions

Based on the pilot symbols received along the sideways path by each receiving antenna, all 16 channels are estimated using a total transmit power of 100 mW. The different channel gain magnitudes are approximately Rayleigh distributed but with very different average powers (average taken over the sideways path). The normalized average power levels for the 16 combinations of TX and RX antennas are presented in Table III. Normalization has been performed such that the largest channel gain corresponds to a level of 0 dB. The cumulative

TABLE III
AVERAGE POWER LEVELS [DB] RECEIVED ALONG THE SIDEWAYS PATH USING THE 4×4 SYSTEM. THE VALUES ARE NORMALIZED WITH RESPECT TO THE STRONGEST SIGNAL.

TX Antenna	RX Antenna			
	1	2	3	4
1	-4.3735	-3.7644	-1.6813	-1.9287
2	-1.5459	-3.3517	-1.3549	0
3	-7.8781	-6.8867	-6.2397	-6.3283
4	-6.0189	-6.0171	-4.2969	-4.6648

distribution of the instantaneous $E_b/N_0 = SNR_D(\mathbf{H})/2$ at the input of the detector is displayed in Fig. 5, for $N = 1, 2, 4$.

The individual CDFs for the 16 possible 1×1 cases are displayed, with the median case shown in bold. Similarly, for 2×2 diversity, 36 combinations of 2 transmitting antenna ports with 2 receiving antenna ports are possible; all of them are displayed in the graph, with the median CDF as a bold line. The median case is selected based on the median 10% outage probability levels for each individual case.

The rightmost thick line displays the CDF for 4×4 diversity. We observe that in our measurement the 4×4 diversity performs significantly better than any possible combination using 2×2 diversity and certainly better than the median realization for 2×2 diversity.

Based on Fig. 5, the performance gain w.r.t. the 1×1 system is quantified by comparing the 10% outage probability power levels, [8]. These power levels define the 10th percentile in the CDF; the power will be higher than these values 90% of the time. Comparing these values, the 4×4 and median 2×2 systems perform better than the median 1×1 system by 15.0 dB and 9.9 dB, respectively. Note that the results apply to transmissions using the same total transmit power level.

Table IV lists the 10% outage probability levels expressed as E_b/N_0 in dB for the best (MAX), worst (MIN) and median diversity cases. The 4×4 system still performs 1.5 dB better than the best 2×2 case and 6.2 dB better than the best 1×1 case. Note that the "best" scenario refers to the specific path walked by the firefighter, for the specific orientations of receive and transmit antennas. In practice, it is impossible to rely on the best scenario, as the movements of the mobile user are not known a priori.

C. Estimated Nakagami parameters for the CDF

The CDF's for all 16 SISO channels were fitted to the Nakagami distribution and the parameters producing the best fit are listed in Table V.

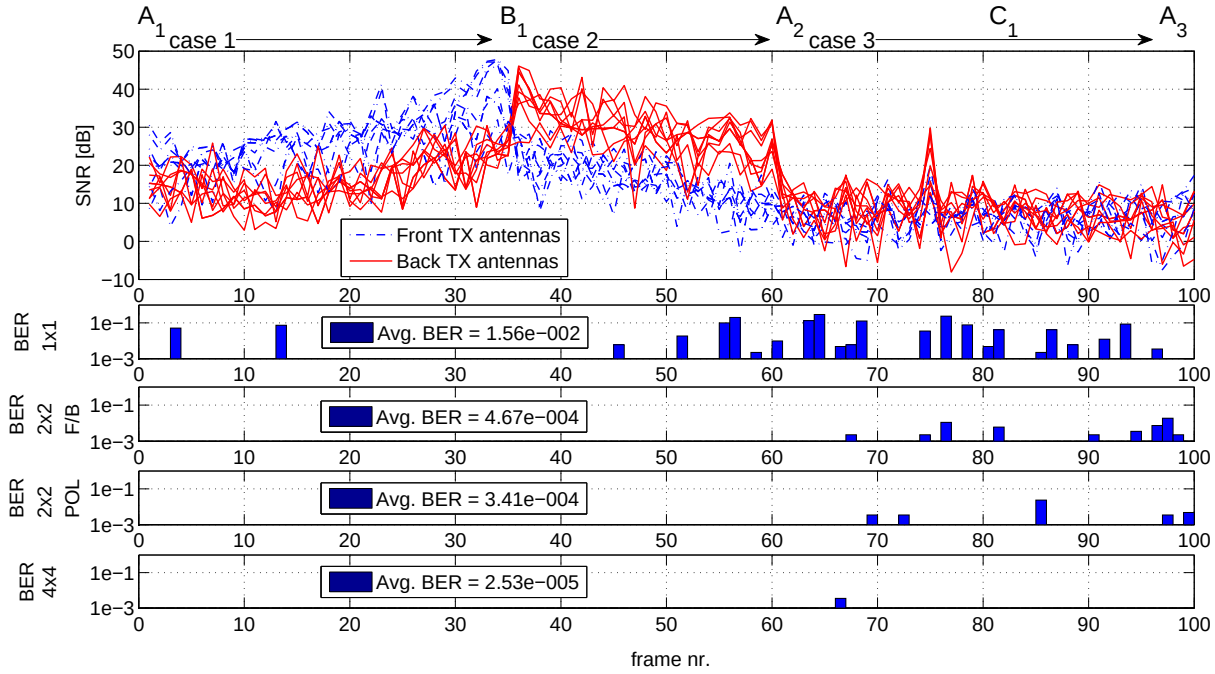

Fig. 4. Signal-to-noise ratios for the 16 channels present in the 4×4 MIMO link. Bit error rates for 1×1, 2×2 front-to-back diversity, 2×2 polarization diversity and 4×4 transmissions (log scale). The transmitted power is chosen very low to create a sufficient number of bit errors for illustration (see text).

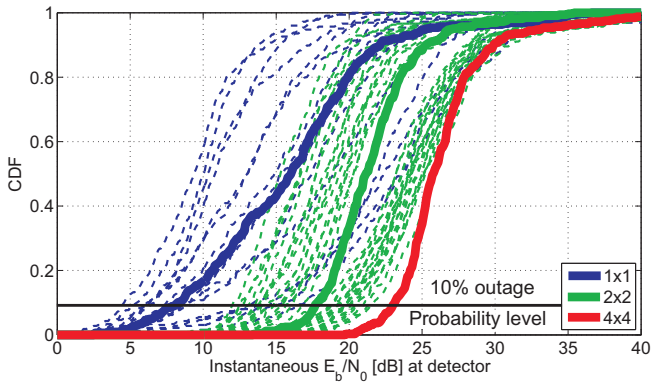

Fig. 5. Cumulative distribution functions for signals measured along the sideways path, from left to right for 1×1, 2×2 and 4×4 links. The CDFs for all possible $N \times N$ combinations are displayed, with the bold lines representing the median $N \times N$ cases, based on 10% outage probability levels.

TABLE IV
MINIMUM, MEDIAN AND MAXIMUM E_b/N_0 FOR 10% OUTAGE PROBABILITY IN THE 1×1,2×2 AND 4×4 CASES MEASURED ALONG THE SIDEWAYS PATH.

SISO/MIMO	1×1	2×2	4×4
N (# cases)	16	36	1
MIN [dB]	4.6	12.1	23.2
MED [dB]	8.2	18.1	23.2
MAX [dB]	17.0	21.7	23.2

The shape factor m varies between 0.7 and 1.8, with an average of 1.06. The actual distribution of a set of measured signals at a specific antenna is the result of a large number of factors, including fading, shadowing (by the body as well as by the environment) and changes in orientation of the antennas.

TABLE V
ESTIMATED NAKAGAMI PARAMETERS FOR THE 16 SISO CHANNELS.

SISO TX-RX	Ω	m
1-1	0.9	0.9
2-1	1.0	0.8
3-1	1.2	1.0
4-1	1.3	0.9
1-2	0.8	1.5
2-2	0.9	1.4
3-2	1.1	1.8
4-2	1.1	1.6
1-3	0.9	0.8
2-3	1.2	0.7
3-3	1.3	0.9
4-3	1.2	1.0
1-4	1.0	0.8
2-4	0.9	0.9
3-4	1.2	1.2
4-4	1.3	0.8

This is consistent with the results obtained in [6], where it was found that a difference in antenna height above the floor level results in different shadowing conditions. Inaccuracies can also result from the limited set of measurements. With on average $m \approx 1$, the signals are considered to be approximately Rayleigh distributed.

Note that the highest m-values occur for the signals related to receiving antenna 2 and/or transmit antenna 3. However, as seen in Table III, the average power levels associated with these antennas are also lower. Therefore the impact of the higher m-values on the bit error characteristics presented in Section III-E will be limited.

The m values are comparable to those listed in [23] for NLoS off-body communication in office environments at 868 MHz.

D. Spatial correlation

Some correlation exists between the signals received from different channels. This correlation is partially caused by the propagation environment and partially by mutual coupling between both feeds of the dual polarized antennas. However, the correlation coefficient is low enough to still achieve a substantial diversity gain by combining the multiple signals [2].

The correlation between the four transmit channel gains $(h_{i,1}, ..., h_{i,4})$ is determined for each of the different receiving antenna ports $(i = 1, ..., 4)$.

For a given port i the correlation for transmit antenna ports (m, n) is defined as

$$\rho_{m,n} = \left| \frac{E\left[h_{i,m} h_{i,n}^*\right]}{\sqrt{E\left[|h_{i,m}|^2\right] E\left[|h_{i,n}|^2\right]}} \right| \tag{4}$$

Table VI displays the channel gain correlation matrices, as seen by each of the four receiver ports. The correlation is higher between signals originating from the same patch antenna and differing only in polarization (values marked in bold). The correlation between front and back signals is lower because the shadowing of the human body isolates the antennas from each other and moreover, their radiation patterns are oriented in opposite directions. For this reason, front to back diversity results in more diversity gain than does polarization diversity. This is confirmed by the bit error characteristics from Section III-E.

TABLE VI
CORRELATION COEFFICIENTS FOR THE TX CHANNEL GAINS, AS RECEIVED BY EACH INDIVIDUAL RX ANTENNA. CORRELATION FOR SIGNALS DIFFERING ONLY IN POLARIZATION IS MARKED IN BOLD.

RX1		TX 1	TX 2	TX 3	TX 4
TX	1	1.00	**0.43**	0.07	0.08
	2	**0.43**	1.00	0.07	0.07
	3	0.07	0.07	1.00	**0.16**
	4	0.08	0.07	**0.16**	1.00

RX2		TX 1	TX 2	TX 3	TX 4
TX	1	1.00	**0.47**	0.05	0.08
	2	**0.47**	1.00	0.04	0.04
	3	0.05	0.04	1.00	**0.16**
	4	0.08	0.04	**0.16**	1.00

RX3		TX 1	TX 2	TX 3	TX 4
TX	1	1.00	**0.32**	0.03	0.11
	2	**0.32**	1.00	0.09	0.10
	3	0.03	0.09	1.00	**0.25**
	4	0.11	0.10	**0.25**	1.00

RX4		TX 1	TX 2	TX 3	TX 4
TX	1	1.00	**0.38**	0.08	0.09
	2	**0.38**	1.00	0.12	0.06
	3	0.08	0.12	1.00	**0.39**
	4	0.09	0.06	**0.39**	1.00

The correlation between the four receiving channel gains $(h_{1,i}, ..., h_{4,i})$ is determined for each of the different transmitting antenna ports $(i = 1, ..., 4)$. For a given port i the correlation for receiving antenna ports (m, n) is defined as

$$\rho_{m,n} = \left| \frac{E\left[h_{m,i} h_{n,i}^*\right]}{\sqrt{E\left[|h_{m,i}|^2\right] E\left[|h_{n,i}|^2\right]}} \right| \tag{5}$$

Table VII displays the correlation matrices of the channel gains $(h_{1,n}, ..., h_{4,n})$ for each of the four transmitting antenna ports $(n = 1, ..., 4)$. As the receiving patch antennas are mounted next to each other at one meter distance, isolation by the body (as for the transmit antennas) is not present here. Moreover the antennas are now oriented in the same direction, providing spatial diversity but no pattern diversity (both antennas now receive signals with similar angles of arrival). Therefore, the correlation between signals from different patch antennas at the receiving side is significantly higher than at the transmitting side. These correlations correspond to the matrix elements $(1, 3)$, $(1, 4)$, $(2, 3)$ and $(2, 4)$.

TABLE VII
CORRELATION COEFFICIENTS FOR THE RX CHANNEL GAINS, FOR SIGNALS TRANSMITTED BY EACH INDIVIDUAL TX ANTENNA. CORRELATION FOR SIGNALS DIFFERING ONLY IN POLARIZATION IS MARKED IN BOLD.

TX1		RX 1	RX 2	RX 3	RX 4
RX	1	1.00	**0.67**	0.48	0.55
	2	**0.67**	1.00	0.53	0.56
	3	0.48	0.53	1.00	**0.68**
	4	0.55	0.56	**0.68**	1.00

TX2		RX 1	RX 2	RX 3	RX 4
RX	1	1.00	**0.43**	0.21	0.50
	2	**0.43**	1.00	0.36	0.44
	3	0.21	0.36	1.00	**0.28**
	4	0.50	0.44	**0.28**	1.00

TX3		RX 1	RX 2	RX 3	RX 4
RX	1	1.00	**0.12**	0.09	0.07
	2	**0.12**	1.00	0.03	0.19
	3	0.09	0.03	1.00	**0.05**
	4	0.07	0.19	**0.05**	1.00

TX4		RX 1	RX 2	RX 3	RX 4
RX	1	1.00	**0.06**	0.06	0.27
	2	**0.06**	1.00	0.13	0.22
	3	0.06	0.13	1.00	**0.26**
	4	0.27	0.22	**0.26**	1.00

Due to the unequal power of the different received signals and the correlation between them, the obtained performance gain will be lower than the theoretical optimum, which is achieved for independent identically distributed fading channels.

However it is clear that the channel gains fluctuate in a partially independent way while the firefighter is walking in the indoor environment. Combining the different received signals will result in a significant improvement of the reliability of the communication, as compared to a 1×1 configuration.

E. Bit error rate characteristics

The BER characteristics can be calculated based on the set of received Signal-to-Noise Ratios $\sigma_s^2 |h_{m,n}|^2 / N_0$. For these calculations only measurement data recorded along the sideways track were used. In this measurement series the path loss is nearly constant. Inevitably some shadowing will be present, making the signal worse than Rayleigh distributed.

Since the measurements were performed with $N_r = N_t = 4$, for the 1×1 and 2×2 links multiple combinations of transmit and receive antenna ports are possible. For a fair comparison, instead of just selecting one possible combination of ports, all possible combinations that yield a given type of diversity are used in the calculation of the BER characteristics.

Assuming the channel amplitude to be approximately invariant during the time of one received burst, the instantaneous bit error rate $BER\left(\mathbf{H}^{(i,j)}\right)$, for the i-th burst and j-th combination of antenna ports, is calculated from (2) and (3) with $\mathbf{H} = \mathbf{H}^{(i,j)}$ where $N = N_t = N_r = 1, 2, 4$ for the diversity cases considered. $\mathbf{H}^{(i,j)}$ is the channel matrix corresponding to the i-th burst and the particular antenna port selection indexed by j.

For example, the four possible antenna port combinations that provide 2×2 polarization diversity are $TX(1,2) \times RX(1,2)$, $TX(1,2) \times RX(3,4)$, $TX(3,4) \times RX(1,2)$ and $TX(3,4) \times RX(3,4)$. The four corresponding 2×2 complex channel matrices include only the complex channel gains which are relevant to the considered combination.

The average BER, averaged over all bursts and all antenna port combinations that yield a given diversity order is calculated as

$$BER = \frac{1}{I \cdot J} \sum_{i=1}^{I} \sum_{j=1}^{J} Q\left(\sqrt{SNR_D\left(\mathbf{H}^{(i,j)}\right)}\right) \tag{6}$$

with I the number of bursts and J the number of signal combinations considered for that particular diversity case.

This BER is expressed as a function of the average $E_{b,rec}/N_0$ per receive antenna port, given by

$$\frac{E_{b,rec}}{N_0} = \frac{E_{b,tr}}{N_0} \frac{E\left[\|\mathbf{H}\|^2\right]}{N^2} \tag{7}$$

with

$$E\left[\|\mathbf{H}\|^2\right] = \frac{1}{I \cdot J} \sum_{i=1}^{I} \sum_{j=1}^{J} \left\|\mathbf{H}^{(i,j)}\right\|^2. \tag{8}$$

The BER characteristics, as a function of $E_{b,rec}/N_0$, are obtained by computing (6) to (8) for a range of $E_{b,tr}$ values.

Fig. 6 shows the resulting BER curves and displays diversity gain as well as array gain.

The curve "no diversity" refers to the average BER for a 1×1 configuration. This characteristic is calculated for the average channel, involving all 16 possible transmit/receive port combinations. The curve for the average channel approximates the theoretical curve for 1×1 communication with a Rayleigh distributed signal.

The theoretical characteristics with diversity are calculated [22, p. 825], by taking into account that there is array gain at the receiver but not at the transmitter, assuming independent identically distributed Rayleigh fading channels, as

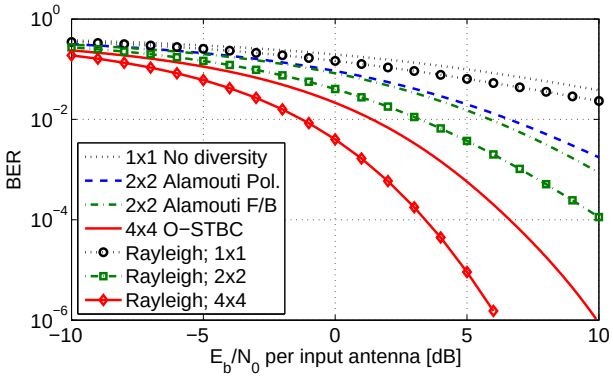

Fig. 6. Bit error graphs showing diversity and array gain. The theoretical characteristics are calculated including receive array gain but no transmit array gain (the total transmitted power is constant).

$$P_b = \left[\frac{1}{2}(1-\mu)\right]^L \cdot \sum_{k=0}^{L-1} \binom{L-1+k}{k} \left[\frac{1}{2}(1+\mu)\right]^k \tag{9}$$

with P_b the bit error probability, L the diversity order and

$$\mu = \sqrt{\frac{E_b/N_0}{L + E_b/N_0}} \tag{10}$$

The use of the Alamouti code to transmit and receive two signals, results in two characteristics for 2×2 MIMO communication. A total of $\binom{4}{2} \cdot \binom{4}{2} = 36$ combinations of 2×2 out of 4×4 channels is possible, of which 4 cases correspond to polarization diversity and 16 cases to pattern diversity (the remaining cases correspond to pattern diversity on one side and polarization diversity on the other side). The BER characteristics are substantially better with 2×2 diversity, but not as good as the theoretical curve for Rayleigh fading with fourth order diversity. Pattern diversity (front-to-back diversity at the transmitter and receiving two signals from different patch antennas) performs better than polarization diversity (transmitting two signals from one patch antenna and receiving two signals in the same way).

Using the orthogonal space-time code for 4×4 MIMO communication results in the largest performance gain. The improvement is, compared to the 2×2 system, very significant. However, the performance is not as good as for the theoretical curve based on Rayleigh fading with 16th-order diversity.

An important conclusion is that the measured characteristics are clearly better for each increase in the order of diversity, illustrating the practical benefits of using transmit as well as receive diversity. In the 2×2 diversity system, front-to-back diversity performs better than polarization diversity, because of the lower correlation between the transmitted signals.

Table VIII displays the $E_{b,rec}/N_0$ ratios in dB needed to obtain a given bit error rate for the recorded signals with varying degrees of diversity. Values marked ($\geq$) are based on the theoretical characteristics for Rayleigh fading, the required E_b/N_0 for the recorded signals will not be smaller.

Due to the absence of a sufficiently large number of channel measurements an accurate calculation for the recorded signals is not possible in these cases. The table clearly illustrates that, using MIMO techniques, a given bit error rate can be achieved using a significantly lower total transmitted power.

TABLE VIII
$E_{b,rec}/N_0$ REQUIRED FOR A GIVEN BER FOR VARYING DEGREES OF DIVERSITY USING THE RECORDED SIGNALS. 2×2 DIVERSITY VALUES FOR POLARIZATION DIVERSITY (POL.) AND FRONT-TO-BACK DIVERSITY (F/B)

	E_b/N_0 [dB]			
BER	1×1	2×2 Pol.	2×2 F/B	4×4
10^{-2}	13.6	6.5	5.8	1.3
10^{-3}	($\geq$23.9)	10.9	9.7	4.4
10^{-4}	($\geq$33.9)	14.8	12.7	6.6

IV. MIMO CHANNEL MODEL

The bit error characteristics in the previous section illustrated that using MIMO techniques, the performance of the system improves significantly compared to a SISO system. However the performance is not as good as predicted by the theory for Rayleigh fading channels with diversity.

The performance of the MIMO system is limited due to the correlation between the channels and the unequal gain of the receiver's four input amplifiers.

Several MIMO channel models that include this correlation are available. In this section two models will be applied to the measurement data recorded along the sideways path.

A. The Kronecker model

The Kronecker model [24], uses separate transmit and receive correlation matrices. The model assumes that the full channel correlation matrix is given by the Kronecker product of the transmitter correlation matrix

$$\mathbf{R}_{TX} = E\left\{\left(\mathbf{H}^H \cdot \mathbf{H}\right)^T\right\} \tag{11}$$

and the receiver correlation matrix

$$\mathbf{R}_{RX} = E\left\{\left(\mathbf{H} \cdot \mathbf{H}^H\right)\right\} \tag{12}$$

as

$$\mathbf{R}_H = \frac{1}{tr\left\{\mathbf{R}_{RX}\right\}} \mathbf{R}_{TX} \otimes \mathbf{R}_{RX} \tag{13}$$

A MIMO channel realization is generated by the model as

$$\tilde{\mathbf{H}} = \frac{1}{\sqrt{tr\left\{\mathbf{R}_{RX}\right\}}} \mathbf{R}_{RX}^{1/2} \mathbf{G} \left(\mathbf{R}_{TX}^{1/2}\right)^T \tag{14}$$

with $tr\{\cdot\}$ the trace of a matrix, $(\cdot)^T$ the transpose and $\otimes$ the Kronecker product.

Theoretically the matrix $\mathbf{G}$ contains i.i.d. random zero-mean complex-normal distributed values. As the distribution of our measured signals is nearly but not exactly Rayleigh distributed this produces a deviation in the characteristics (measured versus modeled channel) of up to 2 dB.

Therefore a $\mathbf{G}$ matrix containing i.i.d. pseudo-random values having the same distribution as the measured signals is generated. The overall distribution of all 5200 signal levels, measured for 16 channels and 325 bursts, is used as a reference for the generation of the matrix.

B. The eigenbeam model

The eigenbeam model [25], treats the influence of the antennas and environment by means of eigenbases and a coupling matrix.

With $\mathbf{U}_A$ and $\mathbf{U}_B$ the eigenbases of the unparameterized one-sided correlation matrices of sides A and B of the link (correlation as perceived from the other side of the link), a MIMO channel realization is generated as

$$\tilde{\mathbf{H}} = \mathbf{U}_A \left(\tilde{\mathbf{\Omega}} \odot \mathbf{G}\right) \mathbf{U}_B^T \tag{15}$$

with $\odot$ the Hadamard (entry-wise) product of $\mathbf{G}$, which is a matrix of i.i.d. random zero-mean complex-normal distributed values, and a coupling matrix $\tilde{\Omega}$.

The coefficients of $\tilde{\Omega}$ specify the mean amount of energy that is coupled from the *m*th eigenvector of side A to the *n*th eigenvector of side B.

C. BER characteristics of the measured and modeled channels

Bit error characteristics are generated for the measured and the modeled channels in a similar way as the one described in Section III-E, however, the BER is now displayed as a function of total E_b/N_0 to show only the diversity gain and not the array gain.

For the measured channels 325 recorded MIMO channel realizations are used. For the channels reconstructed by the models 10^5 realizations are generated, to minimize differences due to the random values in the $\mathbf{G}$ matrix and in this way producing a curve for the average model-based channel realization.

The bit error characteristics are compared to curves for uncorrelated Rayleigh fading to verify the effective diversity order.

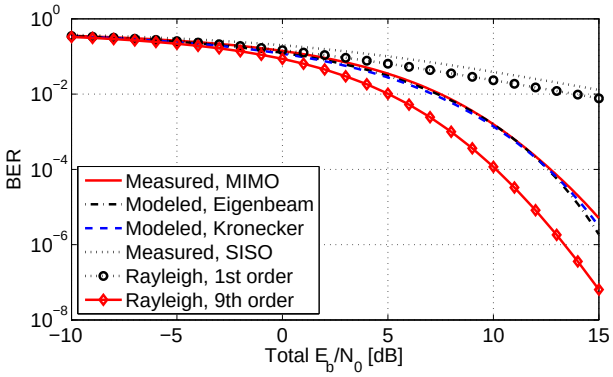

Fig. 7. Diversity gain for the measured and modeled channels, using measurement-like distributed pseudo random values for instantiating the modeled channels.

The associated bit error graphs, displaying the diversity gain, are displayed in Fig. 7 The characteristics display a good match of the models to the measurements, indicating that the correlation properties of the actual MIMO channel were indeed correctly reproduced by both models.

The eigenbeam model, having more parameters, matches the measurements slightly better than the Kronecker model.

V. Performance for different body sizes

To assess the influence of a person's body size, an extra measurement series was performed with three persons of substantially different stature and weight. The results illustrate that the gains obtained by using MIMO techniques are similar for all three persons and also for both measurement campaigns, despite some differences in propagation conditions. The signal distribution is different from the previous campaign as the office environment has changed considerably in the mean time (more equipment and people present). All measurements for this section were performed along the sideways (NLoS) path, in similar operating conditions as the previous measurements.

Fitting the signal values to the Nakagami distribution resulted in the average m-values listed in Table IX, accompanied by the minimum, median and maximum 10% outage probability values.

TABLE IX
Length and weight of the test persons. Best fitting Nakagami-m values for the signal distribution. Minimum, median and maximum E_b/N_0 for 10% outage probability in the 1×1,2×2 and 4×4 cases measured along the sideways path.

Size	Length [m]	Weight [kg]	Nakagami m		SISO/MIMO [dB] 1×1	2×2	4×4
S	1.67	52	0.75	MIN	11.1	21.7	45.2
				MED	26.3	37.7	45.2
				MAX	38.8	45.0	45.2
M	1.75	73	0.83	MIN	12.3	21.2	44.1
				MED	24.8	36.7	44.1
				MAX	37.5	43.8	44.1
L	1.85	104	0.77	MIN	12.8	23.2	46.2
				MED	28.0	38.8	46.2
				MAX	40.0	46.1	46.2

While the distribution of the signal levels is now significantly 'worse than Rayleigh' ($m \approx 0.8$) for all three persons, MIMO communication offers again a substantial performance gain for each increase in the degree of diversity.

Based on the median values and for all three persons, the 2×2 system offers $10.8 - 11.9$ dB of diversity gain, compared to the 1×1 system. Similarly, the 4×4 system offers $15.3 - 18.9$ dB diversity gain, compared to the 1×1 system. These results are similar to those of the previous measurement campaign, with 9.9 dB and 15.0 dB gain for the 2×2 and 4×4 systems, respectively (Section III-B, Table IV).

The BER characteristics in Fig. 8 also display a significant improvement in performance for each increase in the link's diversity order. These results are consistent for all three test persons. A spread of up to 3 dB is present when comparing the BER characteristics for the same diversity order between different test persons. The order of the curves with respect to each other is consistent with the average Nakagami-m values. Some difference is unavoidable as the persons can never walk exactly the same trajectory. For the performance of an off-body communication system in real life, variation in performance is to be expected due to many factors, including the environment, body posture and the specific path followed.

When the antennas are worn at a different height above the floor (due to body size) they consistently experience a slightly different fading pattern, even for a random walk.

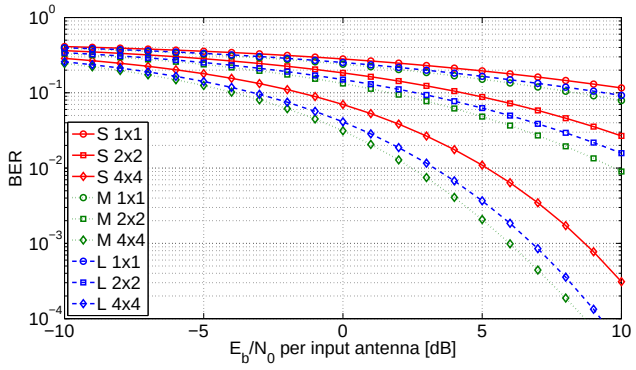

Fig. 8. Bit error graphs for firemen of different sizes, showing diversity and array gain.

Body mass is also not expected to have a significant impact as the torso of even a small adult is still much wider than the size of the antenna patch.

The main conclusion is that for all three persons of different size, MIMO techniques significantly enhance the performance of the wireless link. While the persons experience a different fading distribution, the gains obtained when comparing the 1×1, 2×2 and 4×4 systems are similar. This is the case for both the outage probability levels and the BER characteristics.

VI. Conclusions

The measurements confirm that in a multipath environment, an off-body wireless data link is more reliable when implementing MIMO receive and transmit diversity. The most practical evidence is provided by the bit error rates obtained by demodulation and detection of the data transmitted and received with various orders of diversity. 1×1, 2×2 and 4×4 transmissions were tested, resulting in fewer bit errors for each increase of diversity order, while keeping the transmitted power equal. These BER results include the combination of fading, shadowing, path loss, Doppler spread and channel estimation errors. Cumulative distribution functions allow a comparison of the 10% outage probability levels, providing a quantitative indication of the gain realized by the MIMO system. Measured median gains (relative to a 1×1 system) are 9.9 dB and 15.0 dB for the 2×2 and 4×4 systems, respectively.

Signals with a higher cross correlation provide less diversity gain when combined. However, the correlation coefficients are low enough to achieve a significant performance gain in practice. Bit error characteristics are derived for the different orders of diversity and are compared to theoretical characteristics for Rayleigh fading channels with diversity. In a practical system the diversity gain is compromised due to signal correlation and unequal receiver channel gain.

The off-body MIMO channel was represented by the Kronecker and Eigenbeam models and the bit error graphs were accurately reconstructed from these models.

Additional measurements with persons of different sizes illustrate the MIMO systems consistently increase the performance of the off-body communication link, even for persons of significantly varying sizes.

VII. Acknowledgements

This work was supported by the Fund for Scientific Research - Flanders (FWO-V) by Project "Advanced space-time processing techniques for communication through multi-antenna systems in realistic mobile channels." and by the Postdoctoral Fellowship of H. Rogier.

References

[1] P. Van Torre, L. Vallozzi, C. Hertleer, H. Rogier, M. Moeneclaey, and J. Verhaevert, "Dynamic link performance analysis of a rescue worker's off-body communication system using integrated textile antennas", *Science, Measurement Technology, IET*, vol. 4, no. 2, pp. 41 –52, march 2010.

[2] L. Vallozzi, P. Van Torre, C. Hertleer, H. Rogier, M. Moeneclaey, and J. Verhaevert, "Wireless communication for firefighters using dual-polarized textile antennas integrated in their garment", *Antennas and Propagation, IEEE Transactions on*, vol. 58, no. 4, pp. 1357 –1368, april 2010.

[3] B. Clerckx, C. Craeye, D. Vanhoenacker-Janvier, and C. Oestges, "Impact of Antenna Coupling on 2 x 2 MIMO Communications", *Vehicular Technology, IEEE Transactions on*, vol. 56, no. 3, pp. 1009–1018, May 2007.

[4] C. Oestges, B. Clerckx, M. Guillaud, and M. Debbah, "Dual-polarized wireless communications: from propagation models to system performance evaluation", *Wireless Communications, IEEE Transactions on*, vol. 7, no. 10, pp. 4019–4031, October 2008.

[5] R. Parviainen, J. Ylitalo, R. Ekman, P.H.K. Talmola, and E. Huhka, "Measurement based investigations of cross-polarization characteristics originating from radio channel in 500 MHz frequency", in *Antennas and Propagation Society International Symposium, 2008. AP-S 2008. IEEE*, July 2008, pp. 1–4.

[6] S.L. Cotton and W.G. Scanlon, "Channel characterization for single- and multiple-antenna wearable systems used for indoor body-to-body communications", *Antennas and Propagation, IEEE Transactions on*, vol. 57, no. 4, pp. 980–990, April 2009.

[7] Y. Ouyang, D. J. Love, and W. J. Chappell, "Body-Worn Distributed MIMO System", *IEEE Trans. Vehicular Technology*, vol. 58, no. 4, pp. 1752–1765, May 2009.

[8] Yuehui Ouyang and W.J. Chappell, "Diversity characterization of body-worn textile antenna system at 2.4 GHz", in *Antennas and Propagation Society International Symposium 2006, IEEE*, July 2006, pp. 2117–2120.

[9] I. Khan, P. S. Hall, A. A. Serra, A. R. Guraliuc, and P. Nepa, "Diversity Performance Analysis for On-Body Communication Channels at 2.45 GHz", *IEEE Trans. Antennas Propag.*, vol. 57, no. 4, pp. 956–963, Apr. 2009.

[10] A.A. Serra, P. Nepa, G. Manara, and P.S. Hall, "Diversity measurements for on-body communication systems", *Antennas and Wireless Propagation Letters, IEEE*, vol. 6, pp. 361–363, 2007.

[11] I. Khan and P.S. Hall, "Multiple antenna reception at 5.8 and 10 GHz for body-centric wireless communication channels", *Antennas and Propagation, IEEE Transactions on*, vol. 57, no. 1, pp. 248–255, Jan. 2009.

[12] T.F. Kennedy, P.W. Fink, A.W. Chu, N.J. Champagne, G.Y. Lin, and M.A. Khayat, "Body-worn e-textile antennas: The good, the low-mass, and the conformal", *Antennas and Propagation, IEEE Transactions on*, vol. 57, no. 4, pp. 910–918, April 2009.

[13] Shuai He, X. Dong, Z. Tian, T.C.-K. Liu, M. Ghoreishi, M.L. McGuire, S.W. Neville, and N. Tin, "On the empirical evaluation of spatial and temporal characteristics of ultra-wideband channel", in *Vehicular Technology Conference, 2009. VTC Spring 2009. IEEE 69th*, April 2009, pp. 1–5.

[14] D. Psychoudakis, Gil Young Lee, Chi-Chih Chen, and J.L. Volakis, "Estimating diversity for body-worn antennas", in *Antennas and Propagation, 2009. EuCAP 2009. 3rd European Conference on*, March 2009, pp. 704–708.

[15] D. Neirynck, C. Williams, A. Nix, and M. Beach, "Exploiting multiple-input multiple-output in the personal sphere", *Microwaves, Antennas & Propagation, IET*, vol. 1, no. 6, pp. 1170–1176, Dec. 2007.

[16] J. Karedal, A.J. Johansson, F. Tufvesson, and A.F. Molisch, "A measurement-based fading model for wireless personal area networks", *Wireless Communications, IEEE Transactions on*, vol. 7, no. 11, pp. 4575–4585, November 2008.

[17] M. Hajian, H. Nikookar, F. v. der Zwan, and L.P. Ligthart, "Branch correlation measurements and analysis in an indoor rayleigh fading channel for polarization diversity using a dual polarized patch antenna", *Microwave and Wireless Components Letters, IEEE*, vol. 15, no. 9, pp. 555–557, Sept. 2005.

[18] G. Femenias, "BER performance of linear STBC from orthogonal designs over MIMO correlated Nakagami-m fading channels", *Vehicular Technology, IEEE Transactions on*, vol. 53, no. 2, pp. 307 – 317, march 2004.

[19] L. Vallozzi, H. Rogier, and C. Hertleer, "Dual Polarized Textile Patch Antenna for Integration into Protective Garments", *IEEE Antennas Wireless Prop. Lett.*, vol. 7, pp. 440–443, 2008.

[20] SM Alamouti, "A simple transmit diversity technique for wireless communications", *Selected Areas in Communications, IEEE Journal on*, vol. 16, no. 8, pp. 1451–1458, 1998.

[21] C. Oestges and B. Clerckx, *MIMO Wireless Communications: From Real-World Propagation to Space-Time Code Design*, Academic Press, 2007.

[22] J.G. Proakis et al., *Digital Communication*, Osborne-McGraw-Hill, 2001.

[23] SL Cotton and WG Scanlon, "Characterization and Modeling of the Indoor Radio Channel at 868 MHz for a Mobile Bodyworn Wireless Personal Area Network", *Antennas and Wireless Propagation Letters*, vol. 6, 2007.

[24] J.P. Kermoal, L. Schumacher, K.I. Pedersen, P.E. Mogensen, and F. Frederiksen, "A stochastic MIMO radio channel model with experimental validation", *Selected Areas in Communications, IEEE Journal on*, vol. 20, no. 6, pp. 1211–1226, Aug 2002.

[25] W. Weichselberger, M. Herdin, H. Ozcelik, and E. Bonek, "A stochastic MIMO channel model with joint correlation of both link ends", *Wireless Communications, IEEE Transactions on*, vol. 5, no. 1, pp. 90–100, Jan. 2006.

Patrick Van Torre received the masters degree in Electrical Engineering from Hogeschool Gent, Ghent, Belgium in 1995. For three years he worked as hardware development engineer in the private sector. Since November 1998 he has been active as educator in electronics and researcher in the field of ultrasound technology. He is currently employed by Hogeschool Gent where he teaches theory courses in Analog Electronics, organizes project oriented lab sessions and is involved in public relations activities and hardware development projects for third parties. He is part-time researcher, affiliated with the Department of Information Technology at Ghent University. His current research focuses on body-worn multiple-input multiple-output wireless communication systems.

Luigi Vallozzi was born in Ortona, Italy, in 1980. He received the Laurea degree in electronic engineering from the Universit Politecnica delle Marche, Ancona, Italy, in 2005 and is currently pursuing the Ph.D. degree in electrical engineering at Ghent University, Ghent, Belgium. His research focuses on design and prototyping of antennas for wearable textile systems, and the modeling and characterization of multiple-input multiple-output wireless communication systems.

Carla Hertleer received the M. Sc. degree in textile engineering from Ghent University, Ghent, Belgium in 1990. For three years, she worked in a vertically integrated textile company that produces terry cloth. She worked during 6 years in a bank office but in June 2000, she decided to return to her roots: textiles. Since then, she works as a researcher at the Textile Department of Ghent University. She has given classes in weaving and Jacquard technology, but her recent activities are mainly concentrated on smart textiles, more specifically the research and development of textile sensors for integration in biomedical clothing and textile antennas. The latter research is carried out in collaboration with the Dept. of Information Technology of Ghent University. Her research is carried out in the framework of national and European projects. In 2009 she received her PhD in Engineering at Ghent University, on the research topic of textilebased antennas.

Hendrik Rogier was born in 1971. He received the Electrical Engineering and the Ph.D. degrees from Ghent University, Gent, Belgium, in 1994 and in 1999, respectively. He is currently a Postdoctoral Research Fellow of the Fund for Scientific Research Flanders (FWO-V), Department of Information Technology, Ghent University where he is also Associate Professor with the Department of Information Technology. From October 2003 to April 2004, he was a Visiting Scientist at the Mobile Communications Group of Vienna University of Technology. He authored and coauthored about 50 papers in international journals and about 70 contributions in conference proceedings. He is serving as a member of the Editorial Boarding of IET Science, Measurement Technology and acts as the URSI Commission B representative for Belgium. His current research interests are the analysis of electromagnetic waveguides, electromagnetic simulation techniques applied to electromagnetic compatibility (EMC) and signal integrity (SI) problems, as well as to indoor propagation and antenna design, and in smart antenna systems for wireless networks. Dr. Rogier was twice awarded the URSI Young Scientist Award, at the 2001 URSI Symposium on Electromagnetic Theory and at the 2002 URSI General Assembly. He is a Senior Member of the IEEE.

Marc Moeneclaey received the diploma of electrical engineering and the Ph.D. degree in electrical engineering from Ghent University, Gent, Belgium, in 1978 and 1983, respectively. He is Professor at the Department of Telecommunications and Information Processing (TELIN), Gent University. His main research interests are in statistical communication theory, (iterative) estimation an detection, carrier and symbol synchronization, bandwidth-efficient modulation and coding, spreadspectrum, satellite and mobile communication. He is the author of more than 400 scientific papers in international journals and conference proceedings. Together with Prof. H. Meyr (RWTH Aachen) and Dr. S. Fechtel (Siemens AG), he co-authors the book Digital communication receivers - Synchronization, channel estimation, and signal processing. (J. Wiley, 1998). He is co-recipient of the Mannesmann Innovations Prize 2000. Since 2002, he has been a Fellow of IEEE. During the period 1992-1994, was Editor for Synchronization, for the IEEE Transactions on Communications. He served as co-guest editor for special issues of the Wireless Personal Communications Journal (on Equalization and Synchronization in Wireless Communications) and the IEEE Journal on Selected Areas in Communications (on Signal Synchronization in Digital Transmission Systems) in 1998 and 2001, respectively.

Jo Verhaevert received the engineering degree and the Ph.D. degree in electronic engineering from the Katholieke Universiteit Leuven, Belgium in 1999 and 2005, respectively. He currently teaches courses on telecommunication at the University College Ghent, department of Applied Engineering Sciences, Ghent, Belgium where he also performs research. His research interests include indoor wireless applications (such as wireless sensor networks), indoor propagation mechanisms and smart antenna systems for wireless systems.